Article

Influence of Abrasive Shape on the Abrasion and Phase Transformation of Monocrystalline Silicon

Junqin Shi [1], Xinqi Wei [1], Juan Chen [1], Kun Sun [1,*] and Liang Fang [1,2,*]

[1] State Key Laboratory for Mechanical Behavior of Materials, Xi'an Jiaotong University, Xi'an, 710049, P. R. China

[2] School of Mechanical and Electrical Engineering, Xiamen University Tan Kah Kee College, Zhangzhou 363105, P. R. China

* Kun Sun: sunkun@xjtu.edu.cn; Tel.: +86 29-8266-5479

* Liang Fang: fangl@xjtu.edu.cn; Tel.: +86 29-8266-5479

Abstract: Effect of abrasive shape on the three-body abrasion behaviors of monocrystalline silicon was investigated by Molecular dynamics modelling. The axial ratio of abrasive particle was varied from 1.00, i.e., a complete sphere, to 0.40 to mimic abrasive shape. The particle's movement turns toward sliding from rolling when the axial ratio becomes less than a critical value 0.46. In the abrasion process, the friction force and normal force showed an approximately sinusoid-like fluctuation for the rolling ellipsoidal particles, while the front cutting of particle caused that friction force increased and became larger than normal force for sliding particles. The phase transformation process was tracked under different particle' movement patterns. The Si-II and Bct5 phase producing in loading process can partially transform to Si-III/Si-XII phase and backtrack to original crystal silicon under pressure release, which also occurred in the abrasion process. The secondary phase transformation showed difference for particles' rolling and sliding movements after three-body abrasion. The rolling of particle induced the periodical and inhomogeneous deformation of substrates, while the sliding benefited producing high-quality surface in CMP process. This study aiming to construct more precise model to understand the wear mechanism benefits evaluating the MEMS wear and CMP process of crystal materials.

Keywords: three-body abrasion; phase transformation; monocrystalline silicon; abrasive shape; molecular dynamics

1. Introduction

Monocrystalline silicon (Si), as the key component of micro-electro-mechanical systems (MEMS), has been broadly investigated, recently [1-3]. It is worthy to note that the mechanical characteristics of silicon, especially the relatively poor friction and wear behaviors, severely limit the working stability of MEMS [4,5]. The research showed that in the wear process, the adhesive wear can transform to the abrasive wear because of the accumulation of wear debris between components, which finally leads to the failure of MEMS devices [6,7]. Actually, the three-body abrasion can be used to accurately describe this complicated abrasive wear process. The interaction between abrasive particle and the silicon substrates controls the worn behaviors and mechanisms.

On the other hand, chemical mechanical polishing (CMP) technique is an important intermediate manufacture technology to improve the surface quality [8]. In the CMP process, the slurry is usually comprised of a liquid solution containing specific chemicals and abrasive particles which play a key role in the material polishing. The abrasive particles are usually driven over the wafer surface by the relative motion between the wafer and the pad. Microscopic analysis of polished surfaces manifested that the mechanical effects of slurry occurs as the repeated sliding, rolling, or indentation of abrasive particles against the wafer surface [8-10]. Clearly, it is of substantial importance to deeply understand the abrasive wear behaviors for achieving ideal surface planarization in CMP process.

There have been various methods, such as in-situ experiment, x-ray diffraction, Raman spectroscopy and transmission electron microscopy (TEM), to explore the abrasive wear behavior, especially for the three-body abrasion of silicon materials [4,11-15]. Oliver [16] evaluated various combinations of component factors, such as the size of abrasive particles, type of workpiece and additives, based on CMP results. Su [17] studied the floating polishing process and manifested that the sliding action on particle surface contributed a driving force to produce the material removal, but the rolling action decreased machining efficiency. It was concluded that a slender particle shape is beneficial to strengthening the material removal of CMP process. All those wear models or experiments were proposed from a pure cutting removal mechanism of spherical particles. Actually, the abrasive particles in wear systems are not regular spheres for either wear of MEMS or CMP process. Anantheshwara et al. [11] stressed the dependence of particle movement pattern, including sliding, rolling and their combinations occurring, on the particle geometry in nanoscale three-body abrasion. Fang et al. [18] assumed an ellipsoidal particle as the first approximation to model real particle contours in three-body abrasion. In addition, much effort has been paid for the abrasion properties of monocrystalline silicon at nanoscale by the molecular dynamics (MD) simulation [19-23]. For instance, Sun et al. [24,25] simulated three-body and two-body abrasive wear of monocrystalline silicon with sphere particle in geometry in the nanoscale. They became conscious of the rolling movement of sphere particle and found that the sliding of particle can prevent the large elastic recovery. Hence, different geometries of abrasive particles could change the movement patterns of particles and thereby result in different wear behavior.

Further, the complicated phase transformation and the ambiguous plastic deformation of monocrystalline silicon are avoided in experiments and theory models due to their complexity. The phase transformation of monocrystalline silicon at a relatively small load and the emergence of nanometer twins at a large load were confirmed [19,20]. The simulations on the mechanical properties and deformation mechanism of silicon indicated the appearance of the metastable phases, Si-II, Si-XII, and amorphous phase during nanoindentation process. Furthermore, several simulated results showed that the Si-I transformed into two types of body-centered-tetragonal phase, i.e. β-Si and Bct5 with fivefold coordination [4,22,23]. The abrasive wear of monocrystalline silicon showed a new phase transformation route, i.e., an initial diamond cubic silicon turned into high density amorphous phase beneath the moving particle and, then transformed into low density metastable amorphous phase in both two-body and three-body abrasion [24,25]. Consequently, phase transformation of monocrystalline silicon is still a research focus due to its complexity and variability, especially in three-body abrasion process, although the most of simulations simplified and even neglected the effect of abrasive particle on the abrasion behavior.

Based on the current status of abrasive wear research, it is necessary to illustrate the role of abrasive geometry contour in the three-body abrasion of monocrystalline silicon. Therefore, the effects of axial ratio of particle on the movement pattern of particle, the interaction between particle and substrates, and the phase transformation of silicon were studied using MD simulation. The ellipsoidal particle was assumed to be an approximation of real abrasive particle and its axial ratio was changed from 1.00, i.e., a complete sphere, to a small value 0.40 at which the particle is a reasonable oblate spheroid. The damage degree of monocrystalline silicon surface was evaluated qualitatively by discussing the phase transformation results and elastic recovery.

2. Simulation model and methodology

MD simulations were performed with LAMMPS code [26]. Figure 1. shows the sandwich model of three-body abrasion. The both two silicon substrates consisted of 292,800 atoms with dimensions of 43.40×8.10×16.30 nm along x-[100], y-[010] and z-[001] directions, and were composed of boundary atom, thermostat atom and Newtonian atom. The boundary layers on the bottom substrate were fixed to be rigid for providing structural stability. The thermostat layers were kept at a constant temperature of 300 K to mimic the heat dissipation in real wear process, while the remaining layers were freely moved according the Newton motion law.

Preprints (www.preprints.org) | NOT PEER-REVIEWED | Posted: 25 December 2017 doi:10.20944/preprints201712.0166.v1

Peer-reviewed version available at Crystals 2018, 8, 32; doi:10.3390/cryst8010032

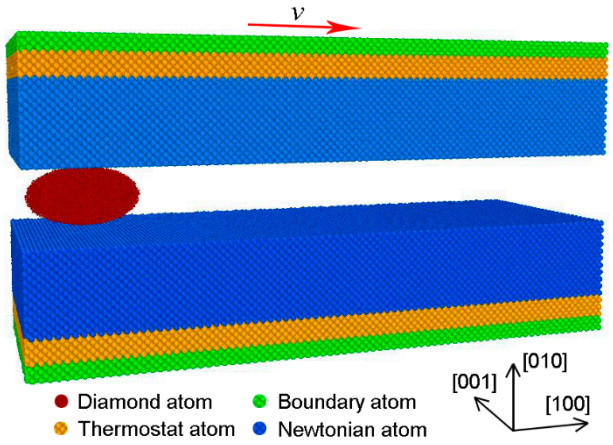

Figure 1. The scheme of initial atomic model of three-body abrasion.

In the CMP process, ceria particles are usually used as abrasive particles with higher hardness compared to monocrystalline silicon [27], which can be treated as rigid particles. In this work, the rigid diamond particles were modeled to facilitate the simulation process. To address the effect of abrasive axial ratio (γ) on the movement pattern of particle and deformed behavior of monocrystalline silicon, the geometry shape of particle varied from complete sphere to ellipsoid with different semi-axes a, b and c. The corresponding parameters of particle are listed in Table 1.

Table 1. Parameters of abrasive particle with different semi-axes a, b and c along x-, y- and z-directions, respectively.

γ = b/a	1.00	0.80	0.60	0.48	0.45	0.40
a (x-axis) /Å	40	40	40	40	40	40
b (y-axis) /Å	40	32	24	19	18	16
c (z-axis) /Å	40	40	40	40	40	40

The interactive force between silicon atoms in the substrates were described by the Tersoff potential [28, 29], and the interactive force between carbon atoms were ignored due to the rigid treatment. The interaction between silicon and diamond particle was depicted with Morse potential [24]:

$$V(r) = D\left(e^{-2\alpha(r-r_0)} - 2e^{-\alpha(r-r_0)}\right) \quad (1)$$

where $V(r)$ is a pair potential energy function, D=0.435 eV is the cohesion energy, α=4.6487 Å^{-1} is relevant to the elastic modulus, r and r_0=1.9475 Å are the instantaneous and equilibrium distance between two atoms, respectively [21,30].

During simulating periodic boundaries were applied in both x- and z-directions, but free boundary was set along y-direction. The equations of motion were integrated with the Velocity-Verlet algorithm with a time step 1 fs. At the beginning, a relaxation process of 100 ps was performed with NVT ensemble and Nose–Hoover thermostat [31,32]. And then, the upper specimen was moved along y-[010] direction to accomplish the constant loading of 80 nN, while the bottom specimen was kept motionless. After the second relaxation of 50 ps, the upper specimen moved horizontally along x-[100] direction on the (010) crystal plane at a constant sliding velocity 50 m/s. The sliding process of the upper specimen was lasted for 1000 ps, corresponding to the sliding distance of 50 nm. During the loading and sliding, all the simulations were carried out at NVE ensemble with the Langevin thermostat to control the temperature of thermostat layer at 300 K.

Preprints (www.preprints.org) | NOT PEER-REVIEWED | Posted: 25 December 2017 doi:10.20944/preprints201712.0166.v1

Peer-reviewed version available at Crystals 2018, 8, 32; doi:10.3390/cryst8010032

3. Results and discussion

3.1. Movement pattern of abrasive particle

The movement pattern of abrasive particle is a very important factor in estimating the materials' wear characteristics [18]. To measure the movement pattern of ellipsoidal particle, we expressed the atomic instantaneous configurations as shown in Figure 2, and the semi-major axis was marked with a white dash line. From Figure 2(a) to (d) showing the change of particles' axial ratio from 1.0 to 0.48, we can find that the position of the marked semi-major axis varied and the rotation angle between the semi-major axis and –x axis varied from 0º to 180º with simulation time. It can be concluded that the particle rolls if the axial ratio is larger than 0.48. When the axial ratio of particle was smaller than 0.48, the particle slid as shown in Figure 2(e) and (f). Resultantly, a particle with smaller axial ratio simulating the sharper particle shows a larger sliding tendency, which is much easier to plough the substrate surface in abrasion process. Furthermore, it is interesting that rolling occurred for the particle with the axial ratio 0.45 at the initial stage as shown in Figure 2(e), and then, the particle slid till the end of simulation process.

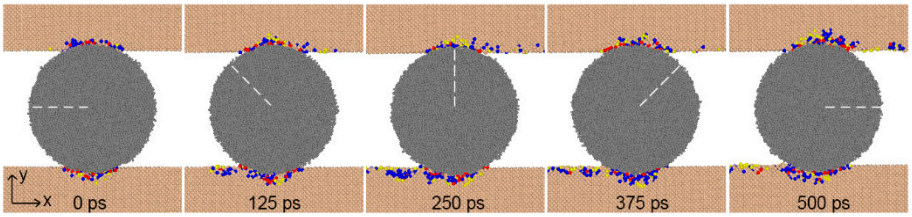

(a)

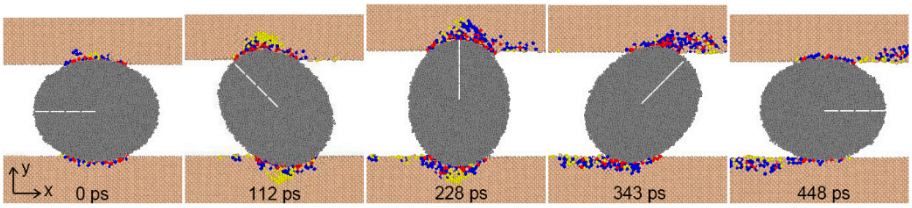

(b)

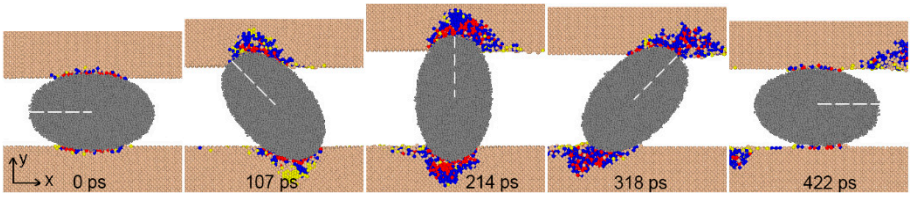

(c)

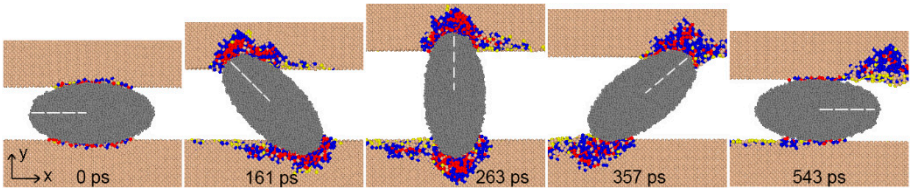

(d)

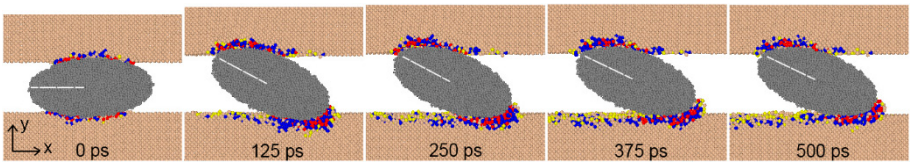

(e)

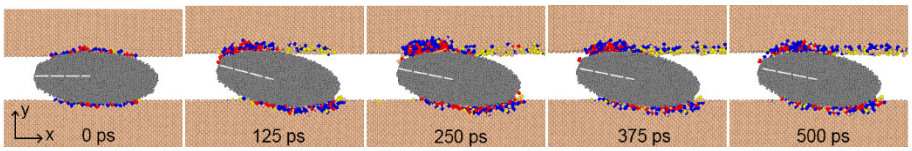

(f)

Figure 2. Atomic instantaneous configurations with different axial ratio (a) 1.00, (b) 0.80, (c) 0.60, (d) 0.48, (e) 0.45 and (f) 0.40. Atoms were colored according to the coordination number: tan, perfect diamond (Si-I) atoms; yellow, Si-III/Si-XII atoms; blue, Bct5 atoms; red, Si-II atoms.

Figure 3 and Figure 4 show the displacement of upper specimen and the angular velocity of abrasive particle, respectively. For sphere particle, both the displacement along y-direction and angular velocity (around 0.6×10-2 rad/ps) were constant. We can also find that the displacement-time curves for particles with the axial ratio 0.80, 0.60 and 0.48 showed sinusoidal curves and their amplitudes increased with the reducing axial ratio. From Figure 4(b) to (d), the positive angular velocity illustrates that the ellipsoidal particle rolled as the axial ratio was larger than 0.48, as shown in Figure 2(b-d). The angular velocity displaying an average fluctuation manifested the rolling movement of particle, namely, the increase in angular velocity demonstrates the particle falls down from the upright posture to the lying in flat, and vice versa. Especially, the angular velocity of the particle with axial ratio 0.48 became very close to 0 around 400-500 ps and 900-1000 ps, meaning the particle tended to sliding over the short period of time. This indicates that the axial ratio 0.48 is close to a critical value causing the change of the particle movement pattern from rolling to sliding. When the axial ratio was less than 0.48, the displacement of upper specimen increased slightly and then kept constant (Figure 3), and in the meantime the angular velocity of particle decreased from a nonzero value to zero (Figure 4(e, f)). This means the beginning of particle sliding need a critical tilt angle (about 22º and 12º for axial ratio 0.45 and 0.40, respectively), which provides the driving force of sliding.

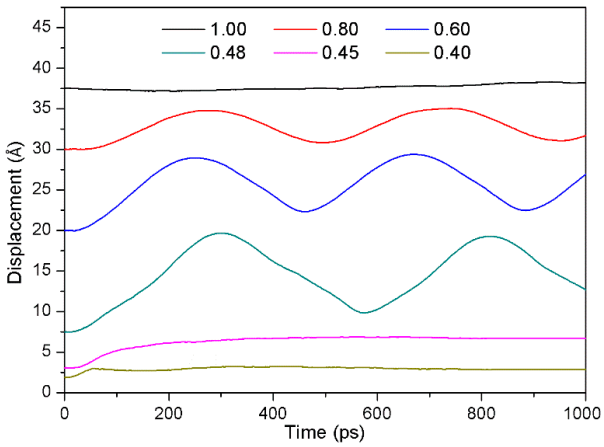

Figure 3. Displacement of the upper specimen along y-[010] direction vs. time and axial ratio. The ordinate value was just used to examine the amplitude of curves.

The prediction of the movement pattern of particle is very important to determine the worn morphology and understand the wear mechanism. Fang et al. have established the criterion of movement pattern of particle to quantify the correlation between theoretical and experimental studies [18,25,33-36], which was described by the following formulas and shown in supplementary material:

$$e/h \geq \mu \quad \text{(for sliding particle)} \qquad (2)$$

$$e/h < \mu \quad \text{(for rolling particle)} \qquad (3)$$

Preprints (www.preprints.org) | NOT PEER-REVIEWED | Posted: 25 December 2017 doi:10.20944/preprints201712.0166.v1

Peer-reviewed version available at Crystals 2018, 8, 32; doi:10.3390/cryst8010032

where $\mu = F/N$ is the coefficient of friction (COF) of particle, e and h is the distance between the central contact point of distributed forces on the particle surface and the geometric center of ellipsoidal particle along x and y direction, respectively.

The e/h was calculated from the modified equation [18], and the forces were assumed equally distributed at the contact zone (ASBC area in Figure S1 in Supplementary Material). Figure 5 shows the e/h curves and COF relative to the simulated time. The e/h was distinctly smaller for the rolling particle than that for the sliding particle, as well as the COF. The average value of COF and e/h as a function of the axial ratio was displayed in Fig 6. Both the e/h and COF increased with the decreasing axial ratio, but the e/h value exceeded μ when the axial ratio was smaller than a critical value 0.46. Consequently, relying on the criterion of movement pattern, there was a critical axial ratio (about 0.46) for ellipsoidal particle in three-body abrasion. When the axial ratio reduced from a large value and then passed over the critical value, the abrasive particle would slide changing from rolling. It is noteworthy that the critical axial ratio maybe varies under different conditions with respect to key parameters such as temperature, normal load and sliding velocity [37,38].

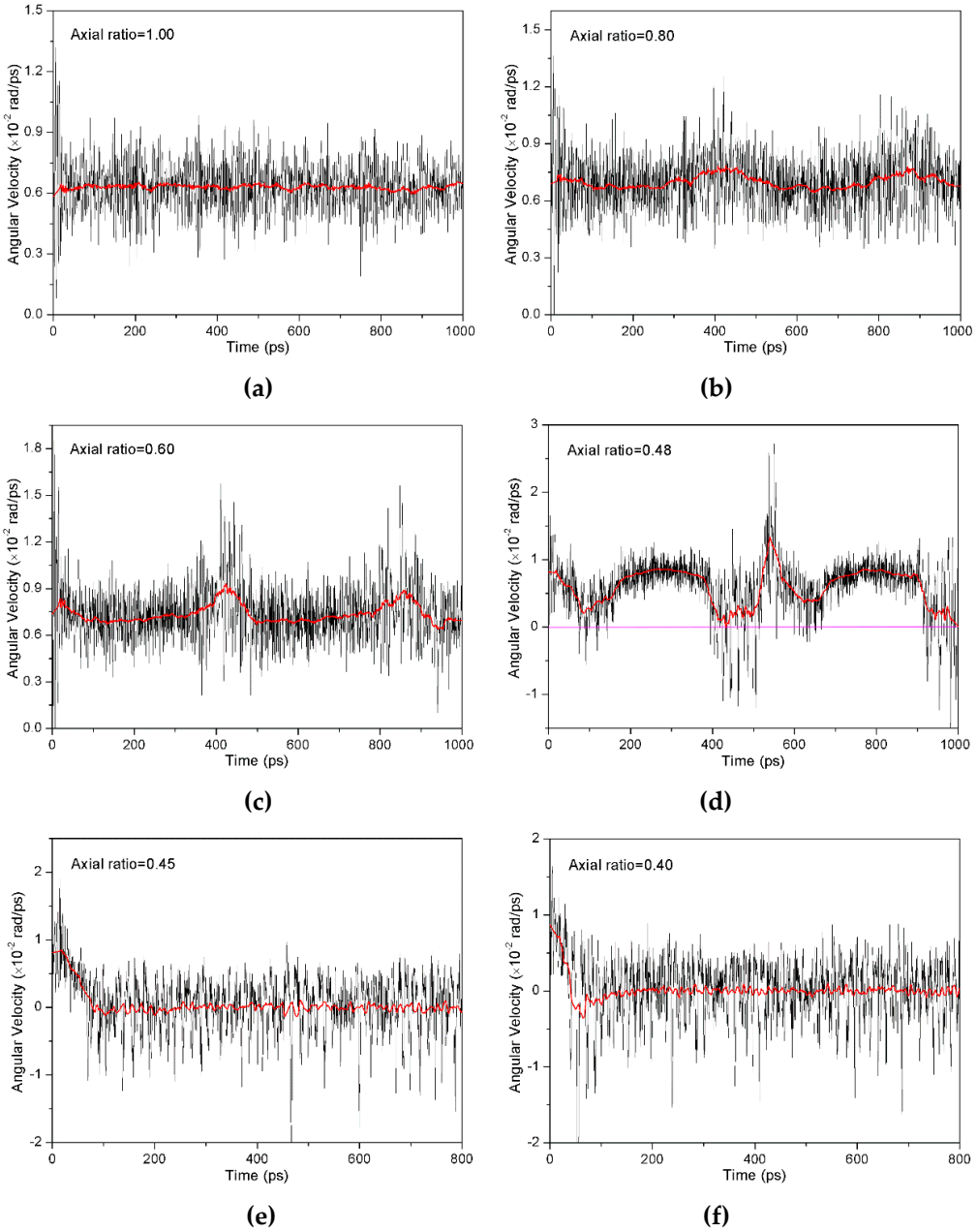

Figure 4. Angular velocity of abrasive center-of-mass vs. time at different abrasive axial ratio.

Furthermore, with the decrease of axial ratio, the friction coefficient increases obviously and even larger than 1.0 for the sliding particle, which is much larger than experimental results. As predicted by macroscale theory, the friction coefficient is comprised of the ploughing and adhesion components [39, 40]. Actually, at the nanoscale, the adhesion friction occurring at the contact regions is very large and even larger than the ploughing friction, and also the contribution of chip or wear debris to friction force cannot be underestimated due to the accumulation of a large number of deformed atoms in front of particle [41]. Therefore, from the perspective of atomic scale, the large friction coefficient is reasonable.

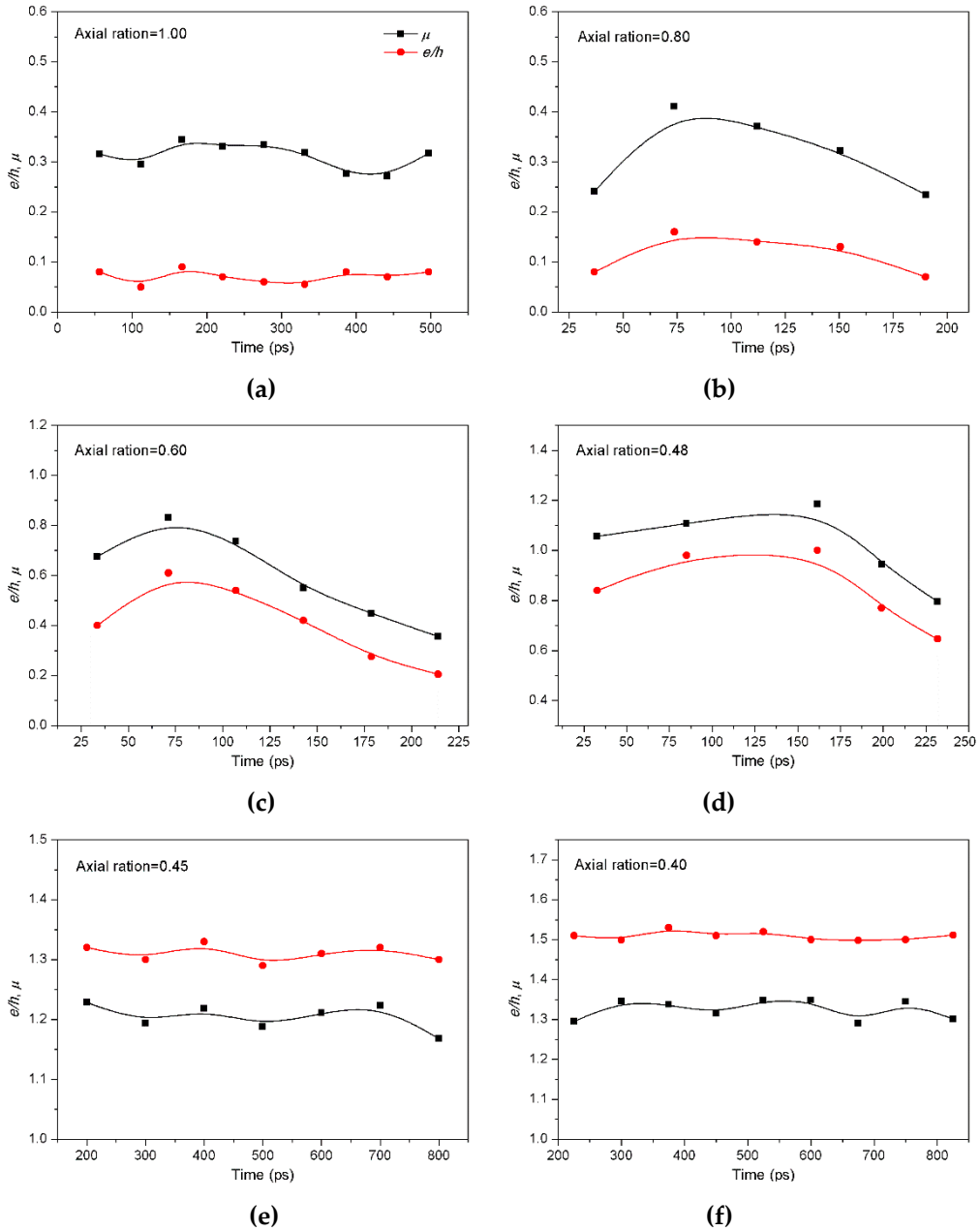

Figure 5. Friction coefficient (μ) and e/h value vs. simulated time at different axial ratio.

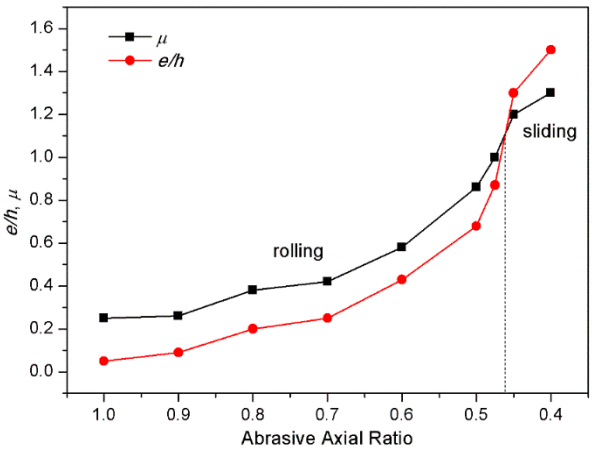

Figure 6. Average friction coefficient (μ) and e/h value at different axial ratio of particles.

It is necessary to analyze the friction force and normal force, as driving and resistant forces, to predict the particles' movement pattern. As shown in Figure 7(a), for the spherical particle which rolled, both the friction force and normal force kept almost unchanged during the abrasion process. For the ellipsoidal particles which rolled, the friction force and normal force fluctuated in sinusoid-like curve approximately at the first half cycle. The curves, however, became much complicated at the second half cycle. When the ellipsoidal particle fell down from upright posture the normal load decreased faster than the friction force. And sometimes normal load changed to negative value for axial ratio from 0.80 to 0.48 due to interatomic attractive force. Friction force was always the driving force and normal force resistant force whether the particle was in the rising or falling stage during rolling. For the sliding particles, as the front of ellipsoidal particle cut the specimen surface, a large number of Si atoms accumulated ahead of particle which increased friction force substantially (see Figure 2(e) and (f)). Hence, the friction force increased significantly and even became larger than the normal force in Figure 7(e) and (f). Similar results have already been reported by others [42].

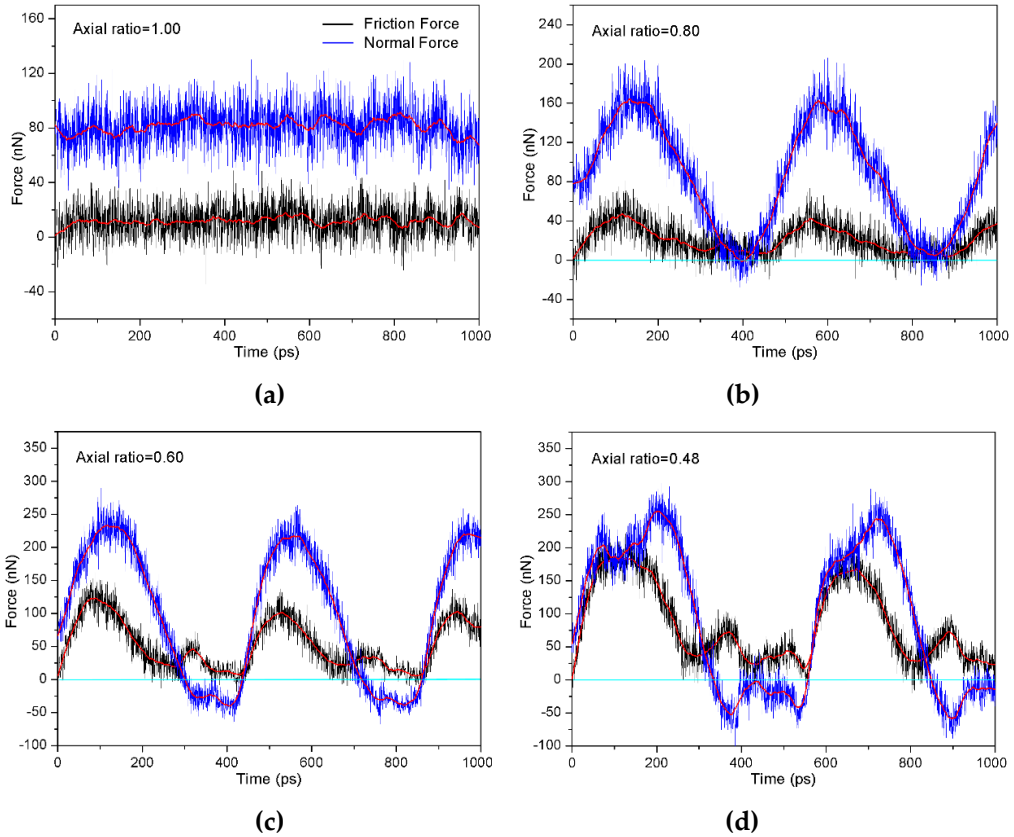

Preprints (www.preprints.org) | NOT PEER-REVIEWED | Posted: 25 December 2017 doi:10.20944/preprints201712.0166.v1

Peer-reviewed version available at Crystals 2018, 8, 32; doi:10.3390/cryst8010032

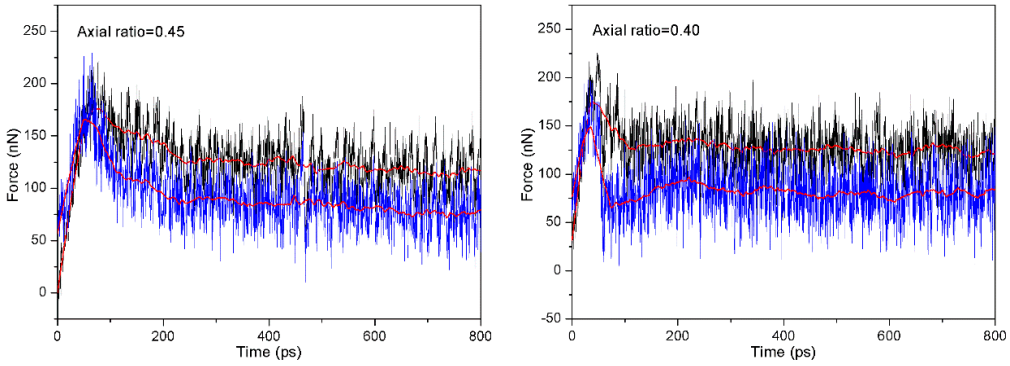

Figure 7. Friction force and normal force vs. time at different axial ratio. Black line is friction force, blue line is normal force and red line is the fitness.

By analyzing the abrasion process, we considered that there exists a critical angle. Once passing over the critical angle, the particle would begin to roll, corresponding to the falling down stage as presented in Figure 2(d). Consequently, at a short period of time, the friction force turned to zero while the repulsive normal force turned to attractive force, as shown in Figure 7(b-d). Those indicate that the particle sharpness reflected by axial ratio can induce the change of interactive force and thereby influenced the movement pattern.

3.2 Phase transformation of monocrystalline silicon

The friction and normal forces vary with the change of abrasive shape as shown in Figure 7, which controls the movement pattern of abrasive particle and then influences the deformation of monocrystalline silicon. Figure 2 shows the different phase transformation behaviors for monocrystalline silicon at different moving stages of ellipsoidal particle. For instance, as ellipsoidal particle is at the upright position the phase transformation is larger in quantity than that in lying posture. Contrarily, the particles with spherical shape or sliding movement cause much less phase transformation in quantity compared with the rolling movement.

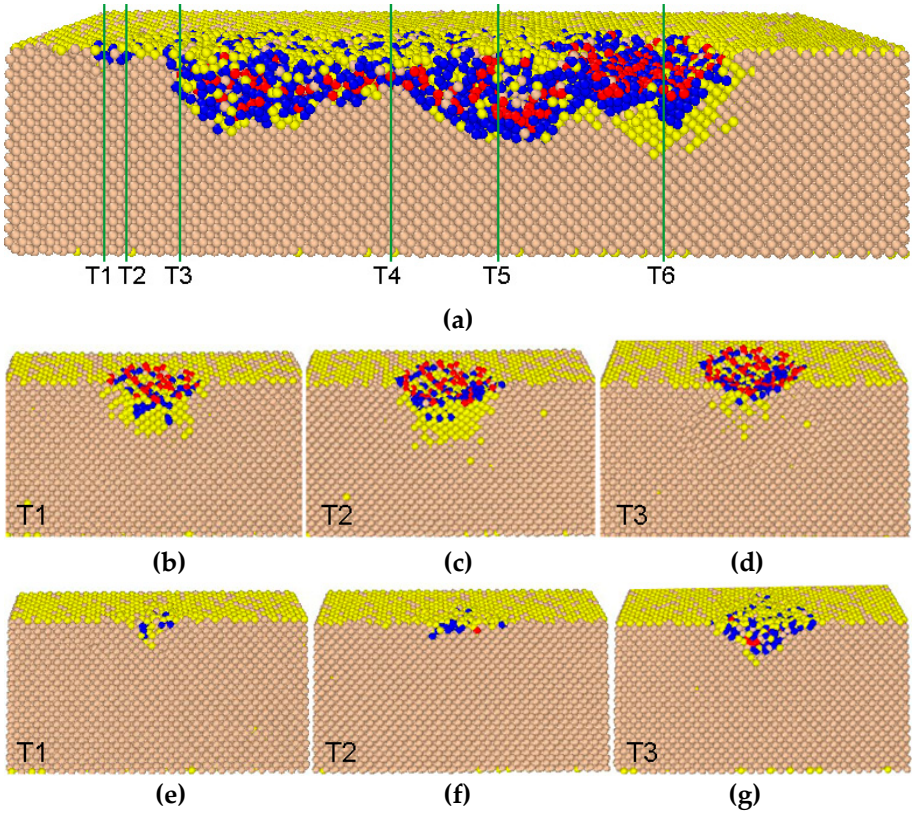

Preprints (www.preprints.org) | NOT PEER-REVIEWED | Posted: 25 December 2017 doi:10.20944/preprints201712.0166.v1

Peer-reviewed version available at Crystals 2018, 8, 32; doi:10.3390/cryst8010032

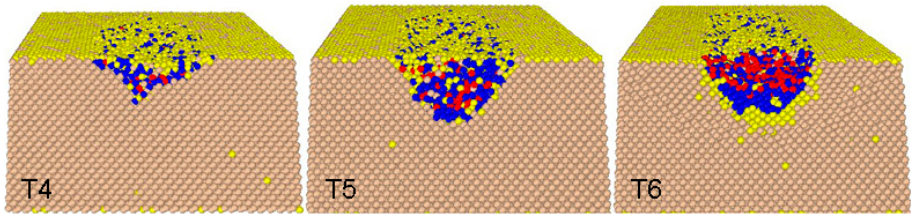

Figure 8. (a), whole cross-section view of phase distribution induced by rolling of particle with axial ratio 0.80; (b-d), cross-section view of initial loading region labelled by T1-T3 before the top substrate moving and (e-g) after the top substrate moving; (h-j), cross-section view of particle lying region (T4), particle upright region (T5) and particle occupying region (T6). Atomic color is similar to that coding in Figure 2.

To further obtain the phase distributions of monocrystalline silicon, the atomic configurations were extracted in Figure 8 and Figure 9 for the particle with axial ratio 0.80 and 0.40, respectively. Different regions on silicon surface were labeled to identify the phase features. In the initial loading region (T1-T3 in Figure 8 and Figure 9(b-d)), the Si-II phase with sixfold coordination and the Bct5 phase with fivefold coordination appeared interactively, some surface atoms (yellow) also appeared and separated the Si-II and Bct5 atoms, and the Si-III/Si-XII phase with fourfold coordination transformed from the initial diamond cubic structure appeared in a deeper position. This phase distribution is somewhat different from the previous observation in which the Si-II phase surrounded by the Bct5 phase occurred at the center and side of the transformational region and a mixed phase of Si-I and Si-III/Si-XII was found beneath the particle [4,24,25]. That is mainly attributed to the small external load of 80 nN resulting in a very shallow indentation in this simulation process. With the particle moving away from the loading region, almost all the phase-transformation atoms disappeared and transformed into the original Si-I atoms again, as shown in (e-g) of Figure 8 and Figure 9. The phase transformation after the particle departing was also confirmed by the atomic number difference in Figure 10. After 20 ps the particle moving off from T3 region, the number differences of phase-transformation Si-II and Bct5 atoms were less than zero whilst that of Si-III/Si-XII was above zero. This indicates that a fraction of Si-II and Bct5 atoms transformed into Si-III/Si-XII atoms rather than Si-I atoms.

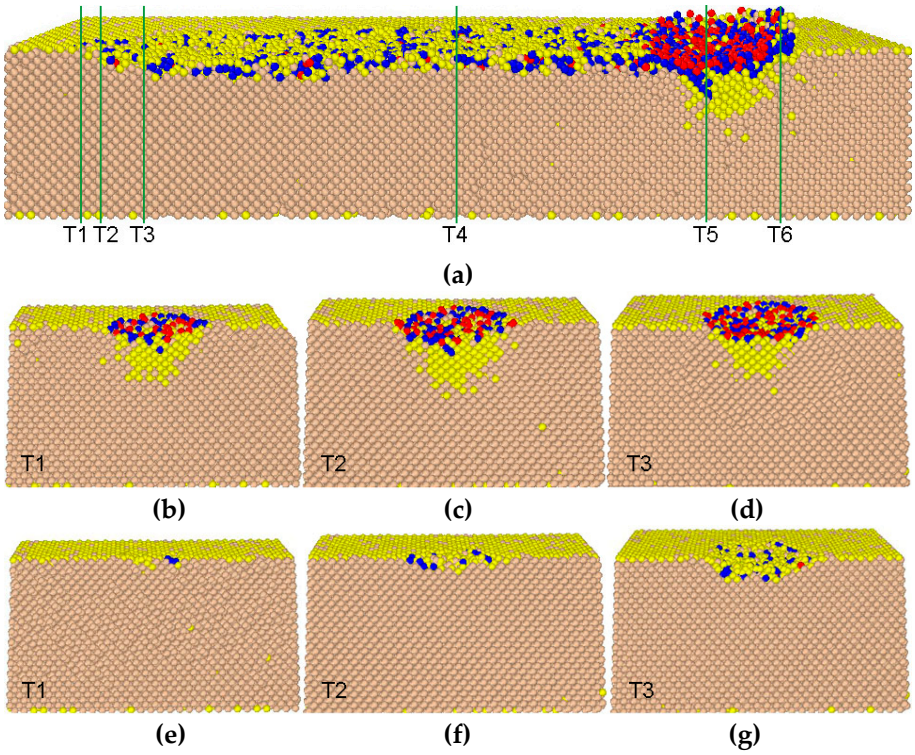

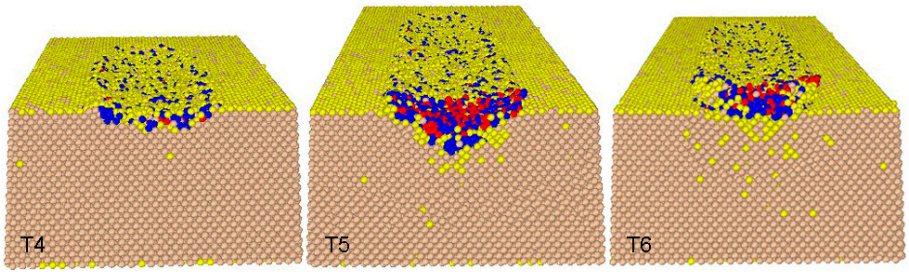

(h) **(i)** **(j)**

Figure 9. (a), whole cross-section view of phase distribution induced by rolling of particle with axial ratio 0.40; (b-d), cross-section view of initial loading region labelled by T1-T3 before the top substrate moving and (e-g) after the top substrate moving; (h-j), cross-section view of particle sliding region (T4) and particle occupying region (T5 and T6). Atomic color is similar to that coding in Figure 2.

For the particle rolling process, the specimen deformation showed a clear difference at different movement stages and exhibited a periodical feature, for instance, the depth of deformed region and the number of deformed atoms for the ellipsoidal particle at upright position (see Figure 8(a) and (i)) were larger than that at lying posture (Figure 8(a) and (h)). However, for particle sliding process, the deformation of specimens was nearly homogeneous in the whole scratched region in Figure 9(a) and (h). The particle with sliding movement pattern could scratch the substrate surface and then lead to more atom accumulation ahead of particle but less deformation within substrate, compared with rolling movement. Consequently, we can find in Figure 8(j) and 9(i, j) that the phase-transformation atoms induced by rolling particle are more than that by sliding particle. Figure 8 (a) and (h-j) show after three-body abrasion, only a part of Bct5 atoms and many Si-II atoms transformed into Si-I or Si-III/Si-XII atoms whilst the other Si-II and Bct5 atoms still remained. Whereas, Figure 9(a) and (h-j) show that the transformation from Si-II and Bct5 phase to Si-I phase increased whilst the remained Si-II and Bct5 atoms were restricted within only several layers in the scratched region, and almost all of Si-III/Si-XII atoms generating from either Si-I or Si-II and Bct5 atoms disappeared because of the pressure releasing. The similar phase transformation phenomena were also observed in two-body abrasion [24,25].

To quantitatively reveal the effect of abrasive shape on the scratched region, we made a statistics of the remaining transformation atom in a range of 25 nm (at least including a whole rolling period) in scratched region at the end of the three-body abrasion, as shown in Figure 11. It can be found that the remaining Bct5 atoms increased dramatically while the Si-II and Si-III/Si-XII atoms showed a slightly increase with the decrease of the axial ratio for rolling particles. However, the decrease of the axial ratio caused a modest reduction of the remaining transformation atoms for particle's sliding process. The statistic data were in good agreement with results in Figure 8 and Figure 9. All those results reveal that particle's sliding movement induces more homogenous surface structure than rolling movement. The geometry of particle with different axial ratio has a significant influence on the plastic deformation of monocrystalline silicon.

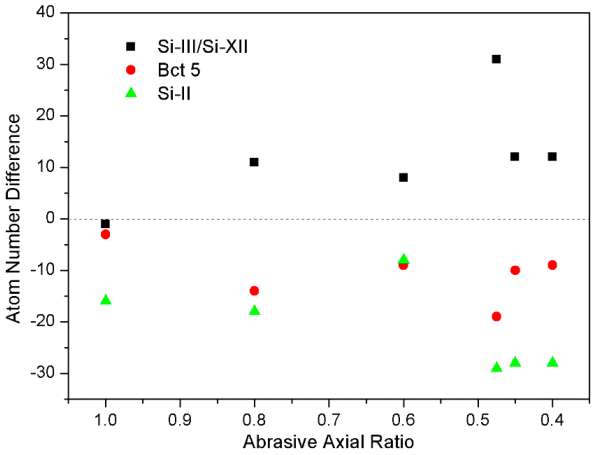

Figure 10. Number difference of the transformational atoms induced by loading to the remaining atoms at the instant of 20 ps from the particle starting to move off.

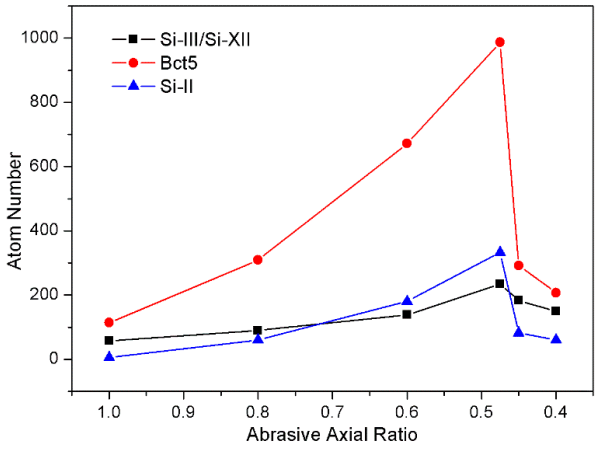

Figure 11. Atom number of the remaining transformation atoms in the scratched region.

4. Damage evaluation of monocrystalline silicon

It is important to evaluate the damage degree of monocrystalline silicon in the three-body abrasion process. Generally, the wear mechanism of materials comprises ploughing and cutting at macro scale [24]. However, the wear or deformation of crystal silicon at nanoscale becomes complicated with effect of abrasive particle shape, as shown in Figure 8-10. From the abrasion configurations as shown in Figure 2, it can be seen that the deformation behaviors of silicon specimens varied at different moving stages of abrasive particle. As ellipsoidal particle is at the upright position the phase transformation was larger in quantity than that in lying posture, and the phase transformation caused by spherical particle or sliding ellipsoidal particles was much less compared with rolling ellipsoidal particles.

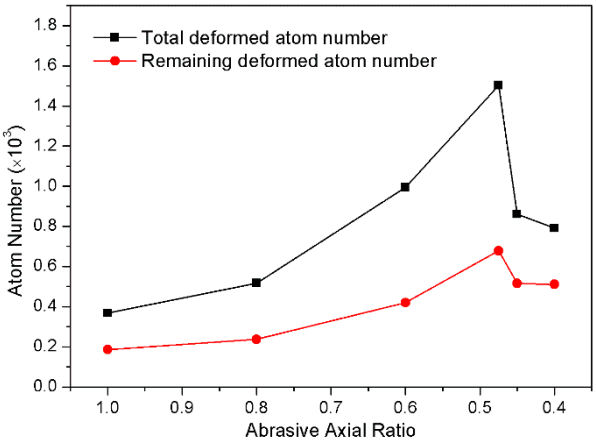

Figure 12. Atom number of the total transformational atoms during the moving process of particles and the remaining transformational atoms in the scratched region.

In Figure 8 and Figure 9, we illustrated the complicated phase transformation which induced the surface damage of monocrystalline silicon and was affected by the particle shape. For the particles' rolling, the total number of phase-transformation atoms in the abrasion process and the number of remaining transformation atoms, in a range of 25 nm in the scratched region, increased with the decrease of the axial ratio, as shown in Figure 12. Meanwhile, Figure 8 shows that the deformation of silicon specimens exhibited an obvious periodicity, i.e., the number of transformational atoms and the depth of deformed region for particle with upright posture were larger than that with lying flat state. Those indicate with the increase in the particle sharpness (i.e., smaller axial ratio) the rolling movement prominently caused the deterioration of surface quality. Whereas, the effects of the axial ratio on the number of transformational atoms (Figure 12) and the depth of deformed region were smaller for particles' sliding movement, and the damage degree of specimen surface was nearly homogeneous in the whole scratched region (Figure 9). Clearly, the rolling process of ellipsoidal particle caused larger surface and subsurface damage.

On the other hand, the elastic recovery was an important factor to influence the abrasion behavior and damage degree of silicon material. We analyzed the evolution of deformed region for both rolling and sliding movement by tracing atomic positions. It can be found that rolling ellipsoidal particle caused a larger substrates deformation than sliding particle. Therefore, the sliding movement of ellipsoidal particle in three-body abrasion benefits producing high-quality surface of monocrystalline silicon wafer.

5. Conclusions

The MD simulation was implemented to investigate the influence of the shape of abrasive particle on the three-body abrasion process of monocrystalline silicon. The varying axial ratio reflecting the sharpness of ellipsoidal particle was used to mimic a real abrasive particle. The results show the particle' rolling movement pattern as the axial ratio decreased from 1.0 (complete sphere) to 0.48 with constant driving of upper specimen. With the axial ratio less than 0.48, the movement of ellipsoidal particle transformed from rolling to sliding. Based on the criterion of movement pattern, the movement pattern of particle can be predicted by comparing the value of e/h and coefficient of friction. The analysis of friction and normal forces indicates that the both two forces fluctuated in sinusoid-like curve approximately for the rolling ellipsoidal particles. As the ellipsoidal particle rolled away from the upright state the friction force turned to zero and the repulsive normal force turned to attractive force. Due to the front cutting of sliding particle, the friction force increased significantly and became larger than the normal force. Then, the phase transformation process of monocrystalline silicon was tracked. The most of Si-II and Bct5 phase, generated in the initial loading process, transformed into original Si-I phase but a part of them transformed into Si-III/Si-XII phase at the early stage of pressure release. During the moving process, the substrate deformation showed

a periodical and inhomogeneous feature for particle's rolling movement but a nearly homogeneous feature for particle's sliding. After three-body abrasion, there were a fraction of Bct5 atoms and lots of Si-II atoms transforming into Si-I or Si-III/Si-XII atoms whilst the other Si-II and Bct5 atoms still remained for the rolling movement. For the sliding movement, there were only several layers of Si-II and Bct5 atoms remaining in the scratched region but the most of them transformed to Si-I atoms. Finally, the damage degree of monocrystalline silicon was evaluated qualitatively by discussing the phase transformation results and elastic recovery. The sliding movement of ellipsoidal particle was beneficial to produce high-quality surface than the rolling.

Furthermore, it is well known that in real CMP process the polishing conditions are very complex, for instance the aqueous slurry consisting of abrasive particles in a mixture of several chemicals has an important effect on the polishing environment. The roughness of the particles also influences the polishing behaviors because the particles have facets or even sub-asperities in real life. Thus, it is necessary to take into account these factors in a more realistic MD scenario to reveal the complex process.

Supplementary Materials: Figure S1: Schematic of forces on an ellipsoidal abrasive particle in three-body abrasion. *A*, *B* and *C* are the contact points between the particle and substrate surface.

Acknowledgments: This work was supported by the National Natural Science Foundation of China [Grant No. 51375364, 51475359] and the Natural Science Foundation of Shaanxi Province of China [2014JM6219].

Author Contributions: Junqin shi, Liang Fang and Kun Sun conceived and designed the simulation, and Junqin Shi wrote the paper; Xinqi Wei performed the simulation; Junqin Shi, Xinqi Wei and Juan Chen analyzed the data".

Conflicts of Interest: The authors declare no conflict of interest.

References

1. Huang, H.; Yan, J.W. New insights into phase transformations in single crystal silicon by controlled cyclic nanoindentation. *Scripta Mater* **2015**, 102, 35–38.
2. Zhang, L.C.; Tang, C.Y. Friction and wear of diamond–silicon nano-systems: Effect of moisture and surface roughness. *Wear* **2013**, 302, 929–936.
3. Zhang. L.; Zhao, H.W.; Yang, Y.H.; Huang, H.; Ma, Z.C.; Shao, M.K. Evaluation of repeated single-point diamond turning on the deformation behavior of monocrystalline silicon via molecular dynamic simulations. *Appl Phys A* **2014**, 116, 141–150.
4. Kim, D.E.; Oh, S.I. Atomistic simulation of structural phase transformations in monocrystalline silicon induced by nanoindentation. *Nanotechnology* **2006**, 17, 2259–2265.
5. Subhash, G.; Corwin, A.D.; de Boer, M.P. Evolution of Wear Characteristics and Frictional Behavior in MEMS devices. *Tribol Lett* **20114**, 1, 177–189.
6. Alsem, D.H.; Dugger, M.T.; Stach, E.A.; Ritchie, R.O. Microscale friction and sliding wear of polycrystalline silicon thin structural films in ambient air. *J Microelectromech S* **2008**, 17: 1144–1145.
7. Shen, S.; Meng, Y.; Zhang, W. Characteristics of the wear process of side-wall surfaces in bulk-fabricated Si-MEMS devices in nitrogen gas environment. *Tribol Lett* **2012**, 47, 455–466.
8. Kasai. T.; Bhushan, B. Physics and tribology of chemical mechnical planarization. *J Phys: Condens Matter* **2008**, 20, 225011.
9. Luo, J.F.; Dornfeld, D.A. Material removal mechanism in chemical mechanical polishing: theory and modeling. *IEEE T Semiconduct M* **2001**, 14, 112–133.
10. Luo, J.F.; Dornfeld D,A. Material removal regions in chemical mechanical planarization for submicron integrated circuit fabrication: coupling effects of slurry chemicals, abrasive size distribution, and wafer-pad contact area. *IEEE T Semiconduct M* **2003**, 16, 45–56.
11. Anantheshwara, K.; Lockwood, A.J.; Mishra, R.K.; Inkson, B.J.; Bobji, M.S. Dynamical evolution of wear particles in nanocontacts. *Tribol Lett* 2012, 45, 229–235.
12. Gupta, M.C.; Ruoff, A.L. Static compression of silicon in the [100] and in the [111] directions. *J Appl Phys* **1980**, 51, 1072–1075.
13. Clarke, D.R.; Kroll, M.C.; Kirchner, P.D.; Cook, R.F. Amorphization and conductivity of silicon and germanium induced by indentation. *Phys Rev Lett* **1988**, 60, 2156–2159.

14. Mann, A.B.; Van, H.D.; Pethica, J.B.; Bowes, P.; Weihs, T.P. Contact resistance and phase transformations during nanoindentation of silicon. *Phil Mag A* **2002**, 82, 1921–1929.
15. Bradby, J.E.; Williams, J.S.; Swain, M.V. In situ electrical characterization of phase transformations in Si during indentation. *Phys Rev B* **2003**, 67, 085205.
16. Oliver, M.R. Chemical mechanical planarization of semiconductor materials (Heidelberg: Springer), 2004.
17. Su, Y.T. Investigation of removal rate properties of a floating polishing process. *J Electrochem Soc* **2000**, 147, 2290–2296.
18. Fang, L.; Zhao, J.; Li, B.; Sun, K. Movement patterns of ellipsoidal particle in abrasive flow machining. *J Mater Process Tech* **2009**, 209: 6048–6056.
19. Zhang, L.; Tanaka, H. Atomic scale deformation in silicon monocrystals induced by two-body and three-body contact sliding. *Tribol Int* **1998**, 31, 425–433.
20. Mylvaganam, K.; Zhang, L.C. Nanotwinning in monocrystalline silicon upon nanoscratching. *Scr Mater* **2011**, 65, 214–216.
21. Du, X.C.; Zhao, H.W.; Zhang, L.; Yang, Y.H.; Xu, H.L.; Fu, H.S.; Li, L.J. Molecular dynamics investigations of mechanical behaviours in monocrystalline silicon due to nanoindentation at cryogenic temperatures and room temperature. *Sci Rep* **2015**, 5, 16275.
22. Eyben, P.; Clemente, F.; Vanstreels, K.; Pourtois, G.; Clarysse, T.; Duriau, E.; Hantschel, T. Analysis and modeling of the high vacuum scanning spreading resistance microscopy nanocontact on silicona. *J Vac Sci Technol B* **2010**, 28, 401–406.
23. Kim, D.E.; Oh, S.I. Deformation pathway to high-pressure phases of silicon during nanoindentation. *J Appl Phys* **2008**, 104, 013502.
24. Sun, J.P.; Fang, L.; Han, J.; Han, Y.; Chen, H.W.; Sun, K. Abrasive wear of nanoscale single crystal silicon. *Wear* **2013**, 307, 119–126.
25. Sun, J.P.; Fang, L.; Han, J.; Han, Y.; Chen, H.W.; Sun, K. Phase transformations of mono-crystal silicon induced by two-body and three-body abrasion in nanoscale. *Comp Mater Sci* **2014**, 82, 140–150.
26. Plimpton, S. Fast parallel algorithms for short-range molecular dynamics. *J Comput Phys* **1995**, 117, 1–19.
27. Chen, Y.; Li, Z.N.; Miao, N.M. Polymethylmethacrylate (PMMA)/CeO_2 hybrid particles for enhanced chemical mechanical polishing performance. *Tribol Int* **2015**, 82, 211–217.
28. Tersoff, J. Modelling solid-state chemistry: interatomic potentials for multicomponent system. *Phys Rev B* **1989**, 39, 5566–5568.
29. Tersoff, J. New empirical model for the structural properties of silicon. *Phys Rev Lett* **1986**, 56, 632–635.
30. Zhao, H.; Shi, C.; Zhang, P.; Zhang, L.; Huang, H.; Yan, J. Research on the effects ofmachining-induced subsurface damages on mono-crystalline silicon via molecular dynamics simulation. *Appl Surf Sci* **2012**, 259, 66–71.
31. Nose, S. A unified formulation of the constant temperature moleculardynamics methods. *J Chem Phys* **1984**, 81, 511–519.
32. Hoover, W.G. Constant-pressure equations of motion. *Phys Rev A* **1986**, 34, 2499–2500.
33. Fang, L.; Zhou, Q.D. A statistical model describing wear traces in three-body abrasion. *Tribotest* **1995**, 2, 47–53.
34. Fang, L.; Kong, X.L.; Zhou, Q.D. A wear tester capable of monitoring and evaluating the movement pattern of abrasive particles in three-body abrasion. *Wear* **1992**, 159: 115–120.
35. Fang, L.; Kong, X.L.; Su, J.Y.; Zhou, Q.D. Movement patterns of abrasive particles in three-body abrasion. *Wear* **1993**, 162, 782–789.
36. Fang, L.; Zhou, Q.D.; Rao, Q.C. An experimental simulation of cutting wear in three-body abrasion. *Wear* **1998**, 218, 188–194.
37. Shi, J.Q.; Chen, J.; Wei, X.Q.; Fang, L.; Sun, K.; Sun, J.P.; Han, J. Influence of normal load on the three-body abrasion behaviour of monocrystalline silicon with ellipsoidal particle. *RSC Advances* **2017**, 7, 30929–30940.
38. Fang, L.; Sun, K.; Shi, J.Q.; Zhu, X.Z.; Zhang, Y.N.; Chen, J.; Sun, J.P.; Han, J. Movement patterns of ellipsoidal particles with different axial ratios in three-body abrasion of monocrystalline copper: a large scale molecular dynamics study. *RSC Advances* **2017**, 7, 26790–26800.
39. Bowden, F.P.; Tabor, D. The Friction and Lubrification of Solids, vol. 1. Clarendon Press, Oxford, 1950–1954.
40. Moore, D.F. Principles and Applications of Tribology. Pergamon, Oxford, 1975.

485 41. Zhu, P.Z.; Hu, Y.Z.; Ma, T.B.; Wang, H. Molecular Dynamics Study on Friction Due to Ploughing and
486 Adhesion in Nanometric Scratching Process. *Tribol Lett* **2011**, 41, 41–46.
487 42. Ren, J.Q.; Zhao, J.S.; Dong, Z.G.; Liu, P.K. Molecular dynamics study on the mechanism of AFM-based
488 nanoscratching process with water-layer lubrication. *Appl Surf Sci* **2015**, 346, 84–98.